This is the accepted manuscript made available via CHORUS. The article has been published as:

Revealing flat bands near the Fermi level in math xmlns="http://www.w3.org/1998/Math/MathML">mrow>mn>1/mn>mi>T/mi>mtext>−/mtext>msub>mi>VSe/mi>mn>2/mn>/msub>/mrow>/math> by using angle-resolved photoemission spectroscopy

T. Yilmaz and E. Vescovo

Phys. Rev. B **105**, L041101 — Published 3 January 2022

DOI: 10.1103/PhysRevB.105.L041101

Revealing flat bands near the Fermi level in 1T-VSe_2 by using angle resolved photoemission spectroscopy

T. Yilmaz and E. Vescovo
National Synchrotron Light Source II, Brookhaven National Lab, Upton, New York 11973, USA
(Dated: December 16, 2021)

Here, we study the surface electronic structure of 1T-VSe_2 by means of angle resolved photoemission spectroscopy and uncover a dispersion-less emission located in the vicinity of the Fermi level. Its crystal momentum dependency reveals that it occupies large portions of the Brillouin zone (BZ), where no bulk band is expected. Upon electron doping (deposition of Rb-atoms), the system evolves in a surprising way. Besides the expected down-shifting of the bands, a splitting of both bulk and dispersion-less emission is observed. This peculiar behavior strongly suggests the intrinsic nature of the dispersion-less emission. Its characterization may therefore be relevant to a deeper understanding of the physics of transition metal dichalcogenides.

Two dimensional (2D) transition metal dichalcogenides (TMDCs) are ideally suited for advanced applications in electronics, spintronics, and optoelectronic [1, 2]. A large number of transition metals and chalcogens provides ample opportunities to synthesize a variety of electronic and crystal structures, supporting complex phenomena such as superconductivity, ferromagnetism, Mott transitions, topological behaviour, and charge density waves (CDW) [3–6]. Therefore, intense experimental and theoretical efforts have been applied to examine the band structure of these materials to reveal novel states of matter. All TMDCs in the 1T-crystal phase share a similar electronic structure, with only minor differences driven by the specific chemical potential [7–9]. Their Fermi surface topology is characterized by ellipsoidal electron pockets dominated by the d-orbitals of the transition metals and centered at the $\bar{M}$-points of the Brillion zone. The $4p$-orbitals of the chalcogen atoms form instead highly dispersive bands which nearly touch the Fermi level at the $\bar{\Gamma}$-point.

Despite their simple band structure, TMDCs have occasionally been shown to host complex and exotic states [10], whose careful experimental determination is therefore of primary importance. Here, we identify a new feature in the prototype dichalcogenide 1T-VSe_2 that has not been realized before. Our angle resolved photoemission spectroscopy (ARPES) experiments reveal that faint, dispersion-less electronic states, located in the vicinity of the Fermi level, cover a large portion of the BZ. The faintness and dispersion-less character with a slowly decreasing density of state towards higher biding energy prevent these features to be clearly resolved in the 2D experimental maps. However, they can be distinguished in the Energy distribution curves (EDCs). Furthermore, surface deposition of Rb atoms leads to the splitting of this band into multiple components. Similar band splitting is also seen in the V-shaped bulk bands dominated by V-3d atomic orbitals. These observations indicate that this emission is correlated with the other bands and cannot be explained by extrinsic factors such as impurities or disorders. We also show that this spectral feature goes beyond the single-particle picture for this system. Our calculated band structure for 1T-VSe_2 is in agreement with previously published calculations and confirms the absence of this band close to the Fermi level in the computed band structure. Hence, this new finding could play an important role in the understanding and engineering of the unique electronic structure of TMDCs.

Single crystal 1T-VSe_2 samples were obtained from 2dsemiconductors (part number : BLK-VSe_2). The ARPES experiments were performed at the 21ID-I ESM beamline at the National Synchrotron Light Source II (NSLS-II), using a DA30 Scienta electron spectrometer with an energy resolution better than 15 meV and linear-horizontal polarized light. The pressure in the photoemission chamber was 310^{-11} torr and samples were cooled by a closed cycle He cryostat and cleaved at 15 K just before collecting the photoemission data. Band structure calculations were performed with the Quantum Espresso (QE) package [11], based on density functional theory without spin-orbit corrections.

The bulk crystal structure of 1T-VSe_2 can be visualized as a stack of 'monolayer'-building-blocks, weakly bonded by van der Waals (vdW) interactions (see Fig. 1 (a)). This system is therefore an ideal 2D material, each building-block comprising a V layer sandwiched between two Se layers. The hexagonal BZ for 1T-VSe_2 is also reproduced in Fig. 1(a) and the computed band structure is displayed in Fig. 1(b). The V and Se contributions to the valence band can be identified by the color coded orbital-character (red/blue for p/d-orbitals). Multiple hole bands, mostly of Se-4p character (red), move towards the Fermi level on approaching the center of the BZ (Γ and A high symmetry points), while the V-3d atomic orbitals (blue) forms relatively flat bands in the vicinity of the Fermi level.

At first sight, the experimental band structure is highly consistent with the calculations. Strongly dispersive bands (Se-4p) and comparably flat bands close to E_f (V-3d orbitals) are indeed the main features seen in the ARPES maps given in Fig. 1(c) and 1(d) in which the calculated band structures are also superimposed. The only difference between the computed and experimental

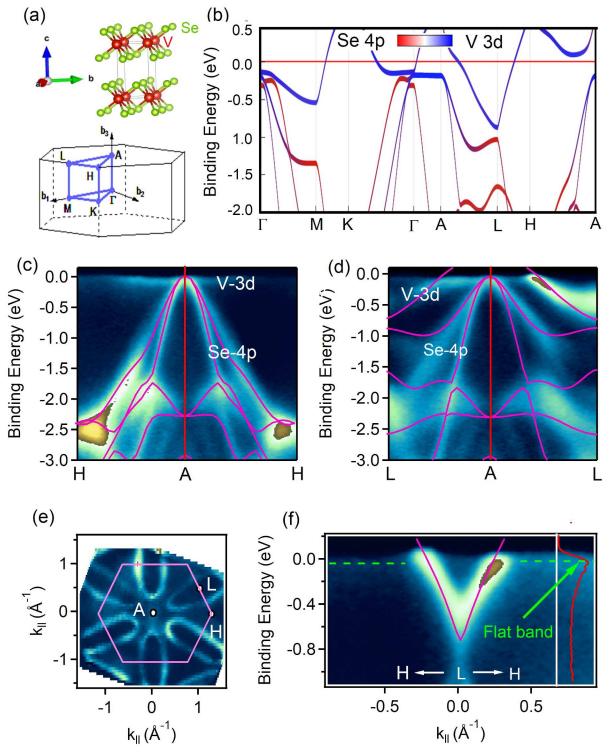


FIG. 1. (a) Ball-and-stick representation of the bulk crystal structure of 1T-VSe_2 and corresponding hexagonal BZ. (b) Calculated band structure with atomic orbital characters. The straight horizontal line at 0 eV marks the Fermi level. (c) - (d) ARPES maps along the A - H and A - L directions. (e) Experimental Fermi surface of 1T-VSe_2. The superimposed hexagon identifies the 2D-BZ. (f) ARPES map along the L - H direction. The EDC away from the V-shaped band is also displayed (red curve) and its peak at the Fermi level is labeled as 'flat band'. The calculated bands (pink curves) are superimposed onto the experimental data in (c), (d), and (f). All spectra were recorded at 15 K with 169 eV photons, corresponding to $k_z \simeq A$-high symmetry point.

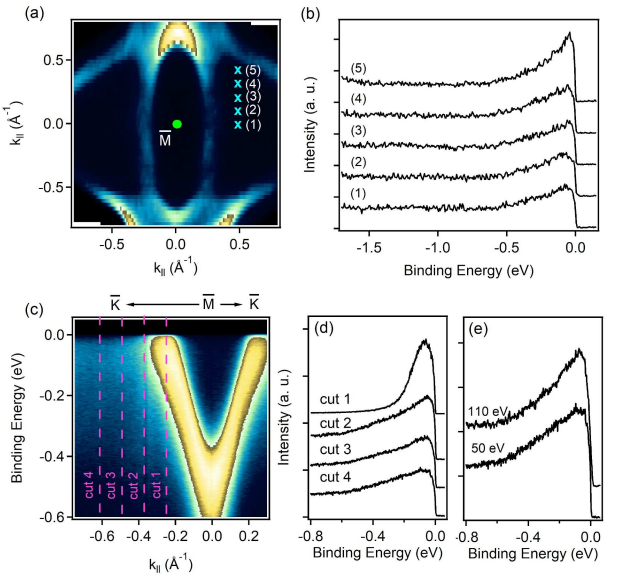


FIG. 2. (a) Portion of the Fermi surface centered at the $\bar{M}$-point. (b) EDCs taken at the momentum points marked in (a). (c) ARPES map centered at the $\bar{M}$-point. (d) EDCs along the dashed pink lines in (c). (e) Photon energy dependent EDCs taken along the momentum point corresponding to the cut 4 in (c). The ARPES maps in (a) and (c) were recorded at 15 K with 50 eV photons.

electronic structure is the slightly higher binding energy of the V-shape 3d band in the calculations. Furthermore, as expected, the experimental Fermi surface is composed of ellipsoidal electron pockets centered at the $\bar{L}$-points (Fig. 1(e)). From the orbital projected band structure, it can be determined that these pockets are dominated by 3d atomic orbitals which form a V-shape band at the L-point (Fig. 1(f)). Thus, our ARPES study captures all the bands predicted by the computational method and these results are identical to earlier observations reported in the literature [12, 13].

Next, we focus on the regions of the electronic structure where no band is supposed to exit. One such region is located about the H-points, outside of the V-shape bulk band. Here, we observe a faint, dispersion-less feature marked with dashed green lines in Fig. 1(f). The interest in this emission, which is barely resolved in the ARPES maps, lies in its peculiar location, away from any predicted energy band (see the regions around the K and H - high symmetry points in the band structure of Fig. 1(b)). This feature is characterized by a spectral bump at the Fermi level with a slowly decreasing intensity towards higher binding energy as seen in the superimposed EDC in Fig. 1(f). The combination of low intensity, weak dispersion, and high broadening makes the detection of this feature quite elusive and can explain why it has not been reported in earlier ARPES studies [12–14].

To further validate our observation, we investigate the energy dispersion along various momentum directions of the 3D-BZ. Several EDCs taken at the marked momentum points in Fig. 2(a) are presented in Fig. 2(b). These points are aligned parallel to the $\bar{M}$ - $\bar{\Gamma}$ direction and are chosen within the region where no band is expected in the vicinity of the Fermi level. In contrast, all EDCs exhibit a peak in the vicinity of the Fermi level with similar line-shape and intensity. Additionally, it is evident from the binding energy of each EDC that this feature forms a flat band. Nominally, V-3d and Se-4p atomic orbitals are strongly dispersive (Fig. 1(b) -1(c)) implying that this feature is not due to secondary electrons from scattering which would mimic the primary electronic dispersion. Similarly, the EDCs taken at various k-points on the $\bar{M}$ - $\bar{K}$ direction, obtained from the ARPES map given in Fig.2(c), display the same spectral line-shape and intensity (Fig. 2(d)). For comparison, in Fig. 2 (d), we also show the EDC taken along the momentum point at the tip of the V-shape bulk band. At the Fermi level, its intensity is only twice the intensity of the flat band.

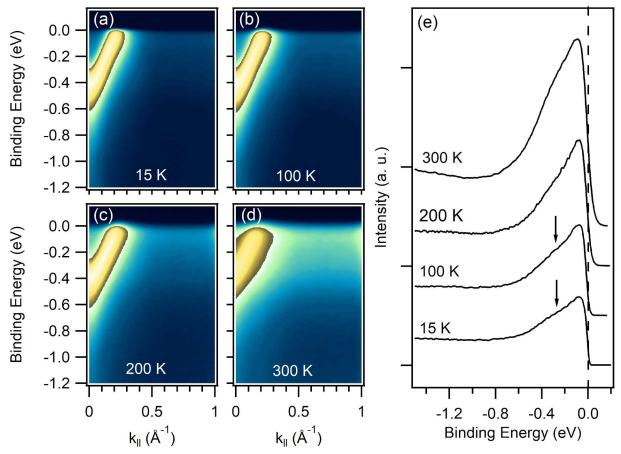


FIG. 3. (a) - (d) Temperature dependency: ARPES maps from 1T-VSe_2 along the $\bar{M}$ - $\bar{K}$ direction. (b) MDCs at $k_{\parallel}$ = 0.6 $\mathring{A}^{-1}$. Spectra were collected with 92.5 eV photons.

However, the spectral shape of the band spreads more towards higher binding energy, possibly indicating the presence of multiple peaks. Therefore, having analyzed two perpendicular directions in the momentum space, we conclude that a flat band covers a large area of 2D-BZ.

In principle, a weak, dispersion-less spectral feature located in the vicinity of the Fermi level and spreading over a large portion of the BZ could be attributed to impurity induced states [15]. To check this possibility, in Fig. 2(e), we compare the EDCs taken with 50 eV, close to the resonant V 3*p*-3*d* transition and with 110 eV photons, far away from resonance. Clearly, the spectral feature of the flat band does not exhibit any prominent dependence on the photon energy, strongly indicating that it does not originate from impurity bands.

Next, we consider the effect of temperature on the flat band. Fig. 3(a) - 3(d) display the ARPES maps of 1T-VSe_2 taken at 15 K, 100 K, 200 K, and 300 K along the $\bar{M}$ - $\bar{K}$ direction. The corresponding EDCs at $k_{\parallel}$ = 0.6 $\mathring{A}^{-1}$ are shown in Fig. 3(e). In these high statistic data, the band clearly reveals its composite nature, with an evident shoulder at higher binding energies, particularly at 15 and 100 K (see arrows in Fig. 3(e)) and less so at higher temperatures, due to thermal broadening. Another interesting observation is that the density of states in the flat band increases with temperature, making its observation quite distinct even in the bare ARPES maps of Fig. 3(e) and 3(d). Such spectral evolution with temperature might indicate a strong electron-phonon coupling for the flat band.

Furthermore, 1T-VSe_2 exhibits CDW phase with a 4 x 4 superstructure. In this case, band folding into the reconstructed Brillouin Zone can induce shadow bands looking like a dispersion-less feature in the experimental band structure. However, temperature dependent ARPES study rules out this scenario since the flat band persist even at room temperature while the CDW in 1T-VSe_2 is present only below 80 K [16].

The broad line-shape of the flat band suggests the presence of overlapping peaks. By breaking the inversion symmetry at the surface, it may be possible to further lift the spin degeneracy or inducing negative electron compressibility in these states [17, 18], thereby making it easier to resolve any underlying substructure. To this end, in the next step, we study the effect of a sub-monolayer Rb deposition on the surface electronic structure of 1T-VSe_2. Our results are shown in Fig. 4 along with the electronic structure of the pristine sample. Surprisingly, instead of a simple band shift due to electron doping, the effect of Rb deposition is a striking modification of the electronic structure (Fig. 4(b)). The first thing to notice is that the original V-shaped band is now split into multiple components marked with red and black dashed parabolas. The band splitting can be easily appreciated in the MDC sections taken at different binding energies. Two distinct peaks are marked with vertical solid lines (red and black, Fig. 4(c)). To better visualize the band splitting, the MDC taken at -0.3 eV binding energy is fitted with Voigt profiles, resolving three distinct features (Fig. 4(d)). The inner two peaks are possibly due to the lifted spin degeneracy while the origin of the outer band remains elusive in our work. On the other hand, the identical MDC taken from the pristine sample exhibits only a single doublet without evident intra-band structure.

Similarly, Rb deposition induces a band splitting in the flat band. Even though this is not very clear in the ARPES map given in Fig. 4(b) (see red horizontal arrows), two weak peaks with an energy separation of 0.17 eV marked with upward arrows in Fig. 4(f) can be identified in the EDCs. Compared to the spectra taken from the pristine sample (orange spectra in Fig. 4(f)), the intensity in the higher binding energy side of the EDC increases in the Rb-deposited sample. This further supports the picture of multiple electronic states in the flat band. Surprisingly, another weak band is also observable inside the V shape band located at 0.1 eV binding energy. This can be seen in the EDC taken at the $\bar{M}$-point. All these new spectral features are more evident in the EDCs integrated over a relatively wide momentum window (Fig. 4(g)). Hence, Rb deposition induces simultaneous splitting in the flat band and the V-shape bulk band, further suggesting the intrinsic nature of the flat band.

To the best of our knowledge, such faint and dispersion-less spectral feature, located in the vicinity of the Fermi level, has been predicted only in materials supporting Holstein polarons, characterized by electron-phonon coupling limited within few atoms (short-range) or several atoms (long-range) [19–21]. From the band structure point of view, these excitations should manifest as splitting of a continuum parabolic band into subbands separated by energy gaps. In close analogy to the flat band reported here, the edge of these bands displays dispersion-less tails spreading over large portions of the BZ. Furthermore, in the Holstein polaron model, a band

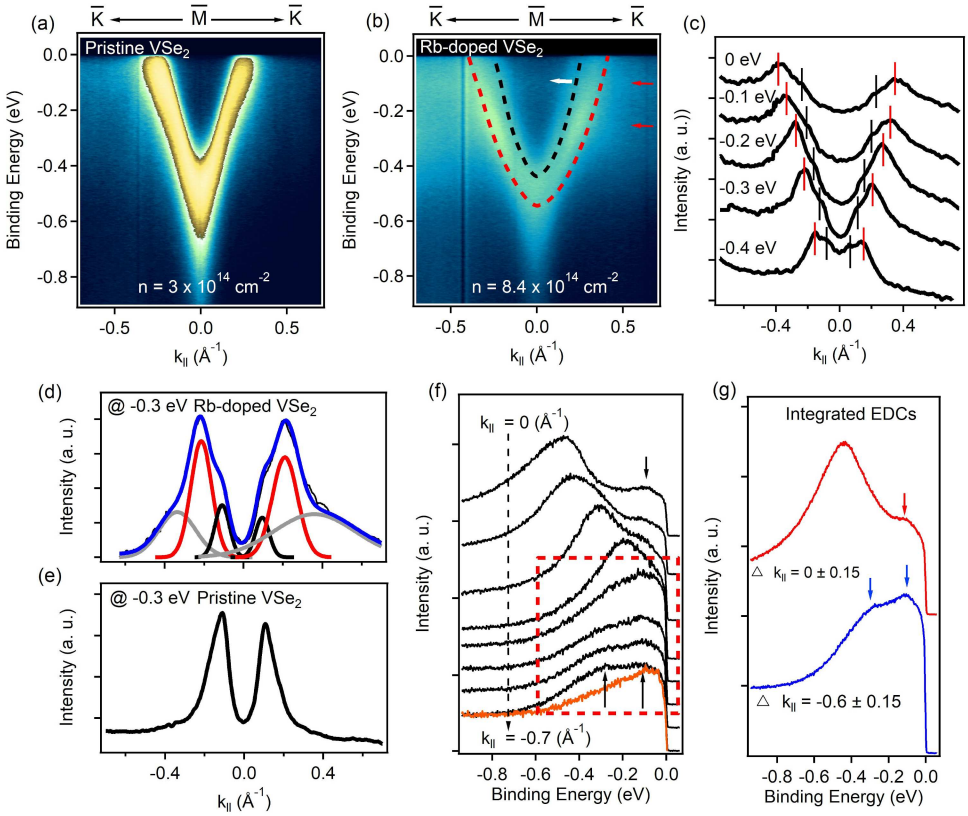


FIG. 4. Rb-deposition: (a) - (b) ARPES map taken from pristine and Rb-deposited 1T-VSe_2, respectively. Black and red parabolas in (b) are guides to the eye. The estimated surface charge densities are also shown, taking into account both states for the Rb doped sample. (c) Momentum distribution curves (MDC) at the indicated binding energies. Black and red vertical lines trace the two bands highlighted in (b). (d) MDC at -0.3 eV binding energy obtained from (b). Black, red, and gray doublets in (d) are Voigt fitting profiles. The overall fitting is the blue curve. (e) MDC at -0.3 eV taken from pristine 1T-VSe_2. (f) EDCs as a function of momentum. The orange spectrum is from the pristine sample for comparison. The red dashed square focuses on the flat band splitting where upward arrows mark the two components. Downward arrow marks the band indicated with a white arrow in (b). (g) Integrated EDCs as specified in fig. Blue and red arrows mark the band locations. Spectra are recorded with 50 eV photons at 15 K.

flattening at the bottom of the sub-bands was also predicted and later confirmed in 2H-MoS_2 through impurity deposition on the sample surface [22]. Similarly, we observe the formation of an additional flat feature inside the V-shape band after the surface deposition of the Rb-impurities (Fig. 4(b)).

Within this scenario, 1T-VSe_2 can be expected to be proximal to superconducting state. Remarkably, this has been found to be the case. A recent work reports on the emergence of superconductivity in 1T-VSe_2 under intense quasi-hydrostatic pressure [23]. The critical temperature for superconductivity is as high as $\sim$4 K at $\sim$15 GPa, which is significantly higher than in any other 1T-TMDC whose origin is attributed to fine-tuning of the chemical potential.

Finally, one of the known characteristics of polarons is the weakness of the quasi-particle peak at the Fermi level [22, 24]. Therefore, direct experimental proof of such electron-phonon coupling may be extremely difficult to obtain. Possibly ultra-high resolution ARPES experiments could be devised to test this scenario. In this connection, we hope that our work can serve as a significant contribution to inspire further investigations aiming at a deeper understanding of the unique electronic anomalies observed in TMDCs and ultimately at better controlling their physical properties.

This research was performed at the ESM (21ID-I) beamline of the National Synchrotron Light Source II, a U.S. Department of Energy (DOE) Office of Science User Facility operated for the DOE Office of Science by Brookhaven National Laboratory under Contract No. DE-SC0012704. We have no conflict of interest, financial or other to declare.

[1] K. F. Mak and J. Shan, Nature Photonics **10**, 216 (2016).
[2] S. Manzeli, D. Ovchinnikov, D. Pasquier, O. V. Yazyev, and A. Kis, Nature Reviews Materials **2**, 1 (2017).
[3] W. Shi, J. Ye, Y. Zhang, R. Suzuki, M. Yoshida, J. Miyazaki, N. Inoue, Y. Saito, and Y. Iwasa, Scientific reports **5**, 1 (2015).
[4] T. Ritschel, J. Trinckauf, K. Koepernik, B. Büchner, M. v. Zimmermann, H. Berger, Y. I. Joe, P. Abbamonte, and J. Geck, Nature physics **11**, 328 (2015).
[5] J. Luxa, O. Jankovskỳ, D. Sedmidubskỳ, R. Medlín, M. Maryško, M. Pumera, and Z. Sofer, Nanoscale **8**, 1960 (2016).
[6] Y.-T. Hsu, A. Vaezi, M. H. Fischer, and E.-A. Kim, Nature communications **8**, 1 (2017).
[7] Y. Chen, W. Ruan, M. Wu, S. Tang, H. Ryu, H.-Z. Tsai, R. L. Lee, S. Kahn, F. Liou, C. Jia, *et al.*, Nature Physics **16**, 218 (2020).
[8] J. Zeb, X. Zhao, S. Ullah, M. G. Menezes, and W. Zhang, Journal of Materials Science **56**, 6891 (2021).
[9] A. M. Woolley and G. Wexler, Journal of Physics C: Solid State Physics **10**, 2601 (1977).
[10] U. Chatterjee, J. Zhao, M. Iavarone, R. Di Capua, J. P. Castellan, G. Karapetrov, C. D. Malliakas, M. G. Kanatzidis, H. Claus, J. P. C. Ruff, *et al.*, Nature communications **6**, 1 (2015).
[11] P. Giannozzi, S. Baroni, N. Bonini, M. Calandra, R. Car, C. Cavazzoni, D. Ceresoli, G. L. Chiarotti, M. Cococcioni, I. Dabo, *et al.*, Journal of physics: Condensed matter **21**, 395502 (2009).
[12] P. M. Coelho, K. Nguyen Cong, M. Bonilla, S. Kolekar, M.-H. Phan, J. Avila, M. C. Asensio, I. I. Oleynik, and M. Batzill, The Journal of Physical Chemistry C **123**, 14089 (2019).
[13] J. Feng, D. Biswas, A. Rajan, M. D. Watson, F. Mazzola, O. J. Clark, K. Underwood, I. Markovic, M. McLaren, A. Hunter, *et al.*, Nano letters **18**, 4493 (2018).
[14] P. Chen, W. W. Pai, Y.-H. Chan, V. Madhavan, M.-Y. Chou, S.-K. Mo, A.-V. Fedorov, and T.-C. Chiang, Physical review letters **121**, 196402 (2018).
[15] J. S. Kang, J. H. Kim, A. Sekiyama, S. Kasai, S. Suga, S. W. Han, K. H. Kim, E. J. Choi, T. Kimura, T. Muro, Y. Saitoh, C. G. Olson, J. H. Shim, and B. I. Min, Physical Review B **68**, 012410 (2003)
.
[16] Giambattista, B., Slough, C., McNairy, W., and Coleman, R., Physical Review B **41**, 10082 (1990)
.
[17] J. M. Riley, W. Meevasana, L. Bawden, M. Asakawa, T. Takayama, T. Eknapakul, T. K. Kim, M. Hoesch, S.-K. Mo, H. Takagi, *et al.*, Nature nanotechnology **10**, 1043 (2015).
[18] M. Kang, B. Kim, S. H. Ryu, S. W. Jung, J. Kim, L. Moreschini, C. Jozwiak, E. Rotenberg, A. Bostwick, and K. S. Kim, Nano letters **17**, 1610 (2017).
[19] W. Li, J. Ren, and Z. Shuai, Nature Communications **12**, 1 (2021).
[20] J. H. Fetherolf, D. Golež, and T. C. Berkelbach, Physical Review X **10**, 021062 (2020).
[21] M. Berciu and G. A. Sawatzky, EPL (Europhysics Letters) **81**, 57008 (2008).
[22] M. Kang, S. W. Jung, W. J. Shin, Y. Sohn, S. H. Ryu, T. K. Kim, M. Hoesch, and K. S. Kim, Nature materials **17**, 676 (2018).
[23] S. Sahoo, U. Dutta, L. Harnagea, A. K. Sood, and S. Karmakar, Physical Review B **101**, 014514 (2020).
[24] N. Mannella, W. L. Yang, K. Tanaka, X. J. Zhou, H. Zheng, J. F. Mitchell, J. Zaanen, T. P. Devereaux, N. Nagaosa, Z. Hussain, and Z.-X. Shen, Physical Review B **76**, 233102 (2007).